ELSEVIER

CrossMark

Chinese Astronomy and Astrophysics 40 (2016) 108–128

CHINESE
ASTRONOMY
AND ASTROPHYSICS

Antenna Performance Measurements at L, S, C, and X Bands for the TM65m Radio Telescope† ⋆

WANG Jin-qing[1,2△] ZHAO Rong-bing[1,2] YU Lin-feng[1,2]
YIN Hai-ling[3] LAO Bao-qiang[1,4] WU Ya-jun[1,2] LI Bin[1,2]
DONG Jian[1,2]
JIANG Yong-bin[1,2] XIA Bo[1,2] ZUO Xiu-ting[1,2] GOU Wei[1,2]
GUO Wen[1,2] WU Xiao-cong[1,2] LU Xue-jiang[1,2] LIU Qing-hui[1,2]
FAN Qing-yuan[1,2] JIANG Dong-rong[1,2] QIAN Zhi-han[1,2]

[1] *Shanghai Astronomical Observatory, Chinese Academy of Sciences, Shanghai 200030*
[2] *Key Laboratory of Radio Astronomy, Chinese Academy of Sciences, Nanjing 210008*
[3] *Shanghai Xinzhuyuan Middle School, Shanghai 200122*
[4] *Guilin University of Electronic Technology, Guilin 541004*

Abstract In this paper, we reported the measured results of the antenna efficiency, sensitivity, and system noise temperature of the TM65m radio telescope. The key parameters describing a radio astronomy receiving system were introduced at first. Then, we discussed the measurement methods and the measuring errors. Finally, the measured results of the antenna efficiency, sensitivity, and system noise temperature performances at the L, S, C, and X bands were given. The results show that the efficiency and SEFD (System Equivalent Flux Density) decrease dramatically at both low and high elevations when the position of the subreflector is fixed. The antenna efficiencies at the C and X bands can be raised to 60% and more in the whole elevation range when the subreflector (servo) model is activated. The system noise temperature is independent to the subreflector model. Among the four wavebands, the C-band sensitivity and system noise temperature are optimal.

† Supported by National Natural Science Foundation (11303076)

Received 2014–09–24; revised version 2014–11–28

⋆ A translation of *Acta Astron. Sin.* Vol. 56, No. 3, pp. 278–294, 2015

△ jqwang@shao.ac.cn

doi:10.1016/j.chinastron.2016.01.010

Key words instrumentation: TM65m radio telescope—methods: radio astronomy

1. INTRODUCTION

The Shanghai TM65m is the greatest fulled-aperture radio telescope in China up to now, its working wavelengths cover the L, S, C, X, Ku, K, Ka, and S eight wavebands, it is the radio telescope with the broadest frequency coverage in this country. The telescope adopts a Cassegrain antenna, the main reflector of 65 m diameter has an active surface adjustment mechanism for compensating its gravity deformation during high-frequency observations. The subreflector of 6.5 m diameter is installed on a 6-pot platform for adjusting its attitude according to the different elevation angle, in order to compensate the displacement of the subreflector relative to the main dish caused by gravity and the supporting arm deformation. At present, this antenna has been equipped with 4 sets of receivers at the L, S, C, and X low-frequency bands, in which, the S/X band is of dual-frequency feed, others are of single-frequency feed.

The antenna efficiency, system noise temperature, and sensitivity are three key-important specifications of a radio telescope. The main factors affecting the efficiency of a paraboloidal antenna are the illumination design on the antenna aperture, the antenna surface accuracy, the blocking of the subreflector and its supporting arms, the antenna pointing error, the ohmic loss of antenna surface, and the ambient noise. The system noise temperature of a radio telescope includes not only the part of the feed and receiver noises, but also the noise of atmospheric radiation from the sky, and the leakage noise of ground radiation. Generally, the total cascade noise of the antenna surface, feed, polarizer, and receiver can be used to assess the noise performance of a microwave antenna system, because that the gain of the cooled low noise amplifier (LNA) can attain 30 dB or higher, the noise from the succeeding cascade will be weakened by a factor of about 1/1000, hence the effect of the succeeding cascade can be neglected. In the field of radio astronomy, the sensitivity of the antenna system is evaluated by the system equivalent flux density (SEFD), which is defined as the ratio of system noise temperature with the antenna temperature per flux unit. Hence, the sensitivity improvement can be realized by reducing the system noise temperature or by increasing the antenna temperature of unit flux.

This paper discussed at first the radio astronomy method to measure the antenna efficiency, then described some noteworthy points in the measurements of efficiency, system noise temperature, and sensitivity, and finally gave the actually measured results of the antenna performances of the TM65m radio telescope at the low-frequency bands. At the same time, the performances at the C and X bands when the subreflector servo model is activated were measured, and some analysis was made on the measured performances.

2. METHOD OF ANTENNA EFFICIENCY MEASUREMENT

In order to measure the efficiency of the radio telescope, we may adopt a radio source of known flux, and measure the power received by the antenna, then compare it with the power received by an ideal paraboloidal surface, this ratio is denoted as $\eta(\varphi)$:

$$\eta(\varphi) = \frac{2kT_{\rm as}(\varphi) K_1K_2K_3K_4K_5}{SA_{\rm g}}, \tag{1}$$

in which, φ is the antenna's elevation angle; k is the Boltzmann constant (1.38065×10^{-23} J/K); $T_{\rm as}$ is the antenna noise temperature (in units of K) caused by the radio source; S is the flux density (in units of Jy) of the radio source at a certain epoch; and the other different factors are defined as follows: K_1 is the correction factor of atmospheric absorption, which is calculated by $K_1 = \frac{V}{\sin\varphi}$, the constant V can be obtained from the curve of atmospheric absorption, namely the value of K_1 is the value of atmospheric attenuation calculated from an atmospheric model; K_2 is the correction factor for the angular size of the radio source, it is assumed to be $K_2 = 1$ for a point source; K_3 is the correction factor for the temporal variation of the radio source flux, if the flux does not vary with the time, then $K_3 = 1$; K_4 is the correction factor for the variation of source flux with the frequency, if the flux does not vary with the frequency, then $K_4 = 1$, otherwise, substituting in the correction curve or consulting the table; K_5 is the correction factor for the polarization of the radio source, when its polarized radiation is negligible, $K_5 = 1$; $A_{\rm g}$ is the geometrical area of the antenna aperture, in units of $\rm m^2$. In the use of the above formula, many errors should be taken into consideration, for a 65 m-class large radio telescope, its beam width is very narrow (only 140" at X-band 8.4 GHz), less than the angular sizes of some radio sources, when the antenna beam points to these sources, only part of source flux is collected, the angular size correction factor K_2 is used just for compensating the loss caused by this reason, however, the determination of K_2 itself has a certain error, and it is the largest error term among all the correction terms[2−4], hence, in the measurement a point source is used as possible in order to avoid the influence of the correction factor. Besides, K_1 is a factor related with the atmosphere and elevation, it is generally obtained by model calculation or by consulting the data table, and this will contribute an error as well. When the above formula is used, it is assumed that the antenna has an ideal pointing performance, in practical measurements, the antenna pointing error should be assessed, and the loss of efficiency caused by the pointing error should be taken into consideration. In addition, the error of source flux is also a factor to cause the measurement error[1]. Table 1 gives the designed efficiency specifications at the four wavebands.

Table 1 The designed efficiency specifications at four low-frequency bands

Band	L	S	C	X
Frequency/GHz	1.3 ∼ 1.8	2.15 ∼ 2.45	4.0 ∼ 8.0	8.0 ∼ 9.0
Best elevation angle efficiency/(%)	55	55	55	55

3. MEASUREMENT OF SYSTEM NOISE TEMPERATURE[5]

The system noise temperature is the cascade of the effective noise temperatures of all the cascaded parts, and simply expressed as:

$$T_{\rm sys} = T_{\rm ant} + T_{\rm feed} + T_{\rm R} + T_{\rm sky} + T_{\rm gnd}, \tag{2}$$

in which, $T_{\rm sys}$ is the noise temperature of the whole antenna system, $T_{\rm feed}$ is the effective noise temperature corresponding to the insertion loss of the feed network (including the polarizer) under the ambient temperature; $T_{\rm R}$ is the noise temperature of the cooled receiver; $T_{\rm sky}$ is the noise temperature from the sky, which enters into the signal channel mainly from the main beam of antenna pattern; T_{gnd} is the ground radiation leakage, which enters into the signal channel mainly from the side lobe and rear lobe of antenna pattern; T_{ant} is the noise temperature caused by the ohmic loss of the antenna surface. It is noteworthy that the expression of Eq.(2) is not restrict, because it has not taken the cascade effect into consideration, it can be approximately used only when the insertion loss of each cascaded part is less than 0.1 dB, the exiting data of measurements indicate that the error caused by this approximate calculation of T_{sys} is ∼0.035 K.

In the centimeter waveband, the Y-factor method is generally used to measure the antenna's system noise temperature, namely, to input at first a white noise signal of known noise temperature into the system, obtaining an output power, then to have the system point to the cold sky, obtaining the second output power, the ratio between the two is the Y factor, from which the system noise temperature can be calculated. At the centimeter waveband, taking the TM65m as an example, the aperture diameters of the feeds at the L, C, S, and X bands are respectively 1.6 m, 0.66 m, 0.91 m, and 0.91 m, but the size of the conventional black body is only about 0.5 m, under the ambient temperature the feed aperture can be covered with one black body by joining multiple black bodies together, this can be realized artificially when the antenna is pointing to the zenith, but this can hardly be realized at the antenna's working elevations. The different input signals can be realized in different manners, recently the cold and hot loads, the cold sky, and calibrated noise source are generally taken as the known input bright temperatures for the measurement. At present, we have adopted the method of calibrated noise source, namely, the noise signal with the known noise temperature T_{cal} is coupled into the system from receiver's LNA front end, then the system noise temperature can be calculated by the proportional formula of Eq.(3):

$$T_{\rm sys} = \frac{P_{\rm b} - P_0}{P_{\rm n} - P_{\rm b}} T_{\rm cal}, \tag{3}$$

in which, P_b is the power reading when the antenna points to the sky background; P_0 is the power reading at the zero point of the receiving system; P_n is the power reading when the antenna points to the sky background, and the noise source is switched on, the proportion in the right side of Eq.(3) is just $1/Y$.

The most significant advantage of this method is that the Y factor can be measured in real time when the antenna points to an arbitrary elevation, and the system noise temperature including the atmospheric noise can be further derived, the disadvantage is that a certain error exists in the noise source calibration. Generally, the calibration of noise source is made by using the cold (liquid nitrogen temperature of 77 K) and hot (ambient temperature 300 K) loads in the laboratory, namely, when the noise source injection is switched off, the feed aperture is covered respectively with the ambient temperature (T_{300}) and liquid nitrogen temperature (T_{77}) loads, which can be realized by putting the black body respectively in the ambient temperature and in the liquid nitrogen, to record the ratio between the power readings corresponding to the two physical temperature inputs, then the Y factor is obtained as follows:

$$Y = \frac{T_{\rm R} + T_{\rm feed} + T_{300}}{T_{\rm R} + T_{\rm feed} + T_{77}}. \tag{4}$$

Hereby, $T_R + T_{feed}$ can be calculated. Then, to switch on the noise source injection, and to repeat the above procedure, thus an other Y factor can be obtained, and a new $(T_R + T_{feed})$ can be calculated, its difference from that obtained when the noise source is switched off gives the calibrated value of the noise injection. The error of this calibration method is about 1∼2 K, and the calibrated value of the noise source may vary with the temperature, it is more apparent for a noise source at the high-frequency band. In order to determine more accurately the calibrated value of the noise source, after the receiver being installed on the antenna, the calibration of noise source made in the laboratory can be further verified by using the Y-factor method composed of the cold sky and ambient temperature load, because that the temperature of the cold sky is lower than 77 K, this Y factor will attain about 10 dB, which is greater than that obtained when the calibration is made in the laboratory with the liquid nitrogen as the cold load, and therefore the calibration error will be smaller. Fig.1 shows the difference between the values of the C-band left-handed polarization noise calibrations made in the laboratory and on the antenna respectively, we can find that below 4.5 GHz, the results of two calibrations are consistent better, as the frequency increases, the difference between the two increases gradually, at the frequencies higher than 6.5 GHz the difference between the two is about 1 K, almost a constant, and their trends of variation with the frequency are completely consistent, at the C-band we have adopted two ranges of noise injections, they are respectively 50% and 5%. In this figure, LCP-High-T_{cal} and LCP-Low-T_{cal} indicate respectively the results of calibrations of left-handed polarization high

and low noise injections made on the antenna site (namely adopting the Y-factor method composed of the cold sky and ambient temperature load), LCP-High-T_{cal}-Lab and LCP-Low-T_{cal}-Lab are those corresponding to the laboratory calibration (namely adopting the Y-factor method composed of the liquid nitrogen 77 K and ambient 300 K loads). In the intervals of 4.2∼4.4 GHz and 5.7∼5.8 GHz, because of the strong external interference, the Y-factor measurement composed of the cold sky and ambient temperature load performs abnormally, but it is in agreement with the laboratory measurement in other frequency ranges.

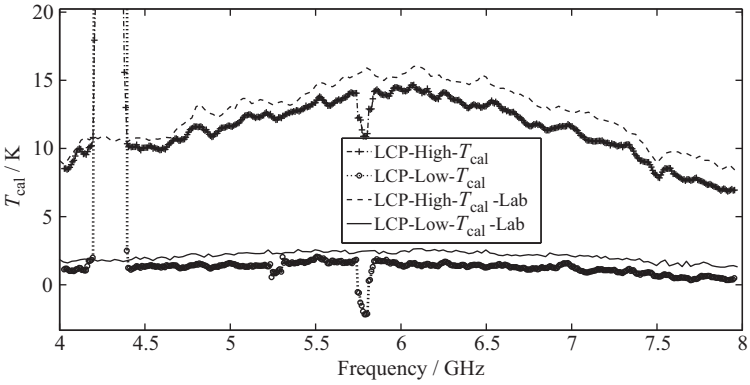

Fig. 1 T_{cal}-values calibrated in the laboratory and on the antenna site

When the Y factor is measured by adopting the cold sky and ambient temperature load, the system noise temperature including the atmospheric noise can be expressed as:

$$T_{\rm sys} = \frac{T_{300}}{Y} + \frac{T_{\rm R} + T_{\rm feed}}{Y}, \tag{5}$$

in which T_{300} is the physical temperature of the ambient temperature load, $T_R + T_{feed}$ is the laboratory-measured value of the receiver and feed noises, and a certain error of which is allowable. Fig.2 gives the effects of the error of $T_R + T_{feed}$ on the value of T_{sys} when the Y factor is as large as 9.5 dB, 10 dB, and 10.5 dB, we can find that for a defined Y factor, even the laboratory-measured $T_R + T_{feed}$ has an error of 9 K, its effect on the final T_{cal} is only 1 K. Generally, the error of laboratory calibration is about 1∼2 K, T_{300} is the physical temperature of the black body under the ambient temperature, with a thermometer its measuring error will be within 0.5 K, so it can be estimated that the actual measurement error of T_{sys} is only about 0.2 K, hence the system noise temperature measured by the Y-factor method composed of the cold sky and ambient temperature load has a very high accuracy (more details about the study and measurement of the system noise temperature can be found in Reference [5]).

4. METHOD OF SENSITIVITY MEASUREMENT

In the field of radio astronomy, the system equivalent flux density (SEFD) is generally used as the assessment specification of sensitivity, this quantity is the ratio of the system noise temperature with the antenna temperature per flux unit (DPFU), the smaller the value of this quantity, the higher the sensitivity. Assuming that the antenna diameter is D, and the efficiency is η, the calculation formulae of DPFU and SEFD are as follows:

$$\mathrm{DPFU} = \frac{A_\mathrm{e} S_\mathrm{U}}{2k} = \frac{\eta\pi D^2 S_\mathrm{U}}{8k}, \tag{6}$$

$$\mathrm{SEFD} = \frac{T_\mathrm{sys}}{\mathrm{DPFU}} = \frac{8kT_\mathrm{sys}}{\eta\pi D^2 S_\mathrm{U}}, \tag{7}$$

in which, A_e is the antenna's effective area, and $S_\mathrm{U} = 1$ Jy is the unit flux density. From Eq.(7) we know that as soon as the system noise temperature and antenna efficiency are defined, the SEFD is determined. The minimum antenna temperature or flux density detectable by a radio telescope can be expressed by the following formulae[6]:

$$\begin{aligned} T_\mathrm{min} &= T_\mathrm{sys}\sqrt{\frac{1}{\Delta f t} + \left(\frac{\Delta G}{G}\right)^2}, \\ S_\mathrm{min} &= T_\mathrm{min}\frac{2k}{A_\mathrm{e}} = \frac{8kT_\mathrm{sys}}{\pi\eta D^2}\sqrt{\frac{1}{\Delta f t} + \left(\frac{\Delta G}{G}\right)^2}, \end{aligned} \tag{8}$$

in which, Δf is the effective bandwidth, t is the integration time, G is the receiver gain, and ΔG is the gain variation. From these formulae we can find that the gain stability of the receiver has a very large effect on the minimum detectable flux density, because it is easy to make the term of $\frac{1}{\Delta f t}$ become very small, but it is difficult to make the gain variation $\frac{\Delta G}{G}$ as small as 1/1000. At present the short-term gain variation can be subtracted by means of periodical noise injection, of course, a certain amount of additional work for data synchronization and derivation is caused.

5. PRACTICAL MEASUREMENTS AND ERROR ANALYSIS

5.1 Theoretical Analysis

In the measurements we have to determine the antenna noise temperature T_{as} caused by the radio source flux, here the calibrated noise source is adopted, the measurement procedures are as follows:

(a) When the antenna points to the cold sky, the power reading is R_b, the corresponding noise temperature is $T_{Re} + T_b$, in which T_{Re} is the equivalent noise temperature of the receiving system, and T_b is the sky background noise, then the system noise temperature is $T_{sys} = \frac{R_b - R_0}{R_N - R_b}$, in which R_0 is the zero point power reading at the terminal end when no

signal is connected to the front end, and R_N is the terminal power reading after the noise source is ignited.

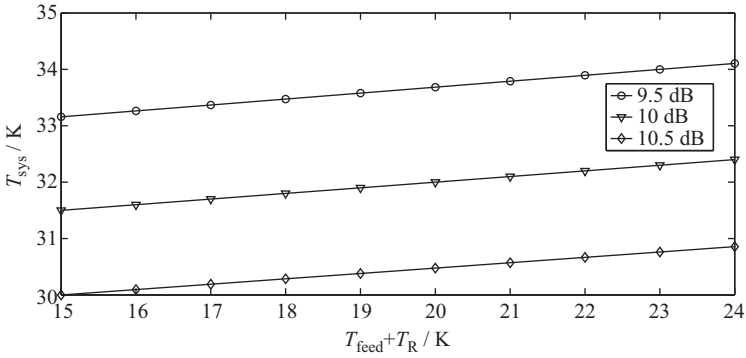

Fig. 2 The receiver and feed noises and the system noise temperature

(b) When the antenna points to a radio source, the power reading is R_S, the corresponding noise temperature is $T_{Re}+T_b+T_{as}$. If the noise source has been precisely calibrated at all frequencies in a broad band, then the calibrated noise source can be used for calculation, on the basis of (a), to ignite the noise tube, then the power reading is R_N, the corresponding noise temperature is $T_{Re}+T_b+T_{cal}$. According to the linear relationship between the power reading and the input power, we have

$$\begin{aligned}(T_{\rm as}+T_{\rm Re}+T_{\rm b})-(T_{\rm Re}+T_{\rm b})&=(R_{\rm S}-R_{\rm b})M,\\(T_{\rm Re}+T_{\rm b}+T_{\rm cal})-(T_{\rm Re}+T_{\rm b})&=(R_{\rm N}-R_{\rm b})M,\end{aligned}\tag{9}$$

in which M is a constant, then $T_{\rm as}=\frac{R_{\rm S}-R_{\rm b}}{R_{\rm N}-R_{\rm b}}T_{\rm cal}$.

(c) Measuring R_S, R_b, and R_N, substituting them into the above formula, and T_{as} is obtained.

(d) By the measured T_{as}, the antenna efficiency can be calculated from Eq.(1). If a point source is used for the efficiency measurement, then the error comes mainly from the measuring error of antenna temperature, the error of radio source flux, the calibration error of the noise source, and the error of the atmospheric correction factor K_1, this can be expressed as

$$\begin{aligned}\frac{\Delta\eta}{\eta}&=\left|\frac{\Delta T_{\rm as}}{T_{\rm as}}\right|+\left|\frac{\Delta S}{S}\right|+\left|\frac{\Delta K_1}{K_1}\right|,\\\frac{\Delta T_{\rm as}}{T_{\rm as}}&=\left|\frac{\partial\ln T_{\rm as}}{\partial R_{\rm b}}\right|\Delta R_{\rm b}+\left|\frac{\partial\ln T_{\rm as}}{\partial R_{\rm N}}\right|\Delta R_{\rm N}+\left|\frac{\partial\ln T_{\rm as}}{\partial R_{\rm S}}\right|\Delta R_{\rm S}+\left|\frac{\partial\ln T_{\rm as}}{\partial T_{\rm N}}\right|\Delta T_{\rm N}\\&=\left|\frac{1}{R_{\rm S}-R_{\rm b}}-\frac{1}{R_{\rm N}-R_{\rm b}}\right|\Delta R_{\rm b}+\left|\frac{1}{R_{\rm N}-R_{\rm b}}\right|\Delta R_{\rm N}+\left|\frac{1}{R_{\rm S}-R_{\rm b}}\right|\Delta R_{\rm S}+\frac{\Delta T_{\rm cal}}{T_{\rm cal}}.\end{aligned}\tag{10}$$

If taking the right-handed polarization of Fig.3 as an example, $R_{\rm b} = 8830$, $\Delta R_{\rm b} = 6$, $R_{\rm N} = 15350$, $\Delta R_{\rm N} = 9$, $R_{\rm S} = 9580$, and $\Delta R_{\rm S} = 8$, the calibration error of the noise tube is assumed to be $\frac{\Delta T_{\rm cal}}{T_{\rm cal}} = 4\%$ ($T_{\rm cal} = 25$ K, $\Delta T_{\rm cal}$ is less than 1 K), then $\frac{\Delta T_{\rm as}}{T_{\rm as}} = 0.059$.

If the flux error of the radio source is $\left|\frac{\Delta S}{S}\right| = 0.005$[7], $\left|\frac{\Delta K_1}{K_1}\right| = 0.05$, then, $\frac{\Delta\eta}{\eta} = \left|\frac{\Delta T_{\rm as}}{T_{\rm as}}\right| + \left|\frac{\Delta S}{S}\right| + \left|\frac{\Delta K_1}{K_1}\right| = 11.4\%$.

If η =0.6, then $\Delta\eta$ =0.06, the measuring error is about 6%. From the above calculation, we can find that $\left|\frac{\Delta T_{\rm s}}{T_{\rm s}}\right|$ and $\left|\frac{\Delta K_1}{K_1}\right|$ are the major part of the error, and the former comes mainly from the calibration error of the noise tube. The practical measurements indicate that when the noise tube that has been calibrated in the laboratory by the cold/hot load method is installed on the antenna, if the measurement adopts directly the laboratory-calibrated value, then a systematic error will be caused (as shown in Fig.1), hence it is necessary to make a verification by using the method of cold sky and ambient temperature load, when the Y factor is greater than 10 dB, the calibration error of this method will be less than that of the laboratory calibration for more than two times. The practical calculation indicates that at the C band the 1 K increase of the T_{cal} value will cause the measured value of antenna efficiency to increase about 8%, and cause the measured value of system noise temperature to increase about 2 K. However, the measurement of SEFD will not be affected by the error of T_{cal}, because that in the process of derivation, the T_{cal} value has been canceled out.

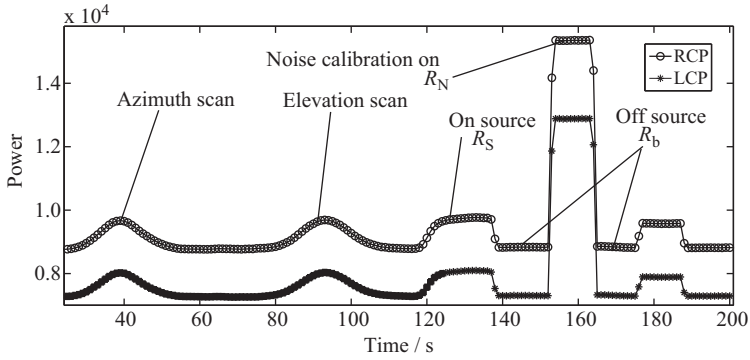

Fig. 3 The measurement record of 3C286 at 8.4 GHz with a 20 MHz bandwidth

5.2 Measurement of Antenna Performances

In order to avoid the influences of the temperature and other environmental factors on the antenna performance measurement, we selected a clear night, and adopted the calibration radio sources 3C286, and 3C123 etc. as the measuring targets, the flux curve of a radio source is shown as Fig.4. The measurements of antenna efficiency, system noise temperature, and sensitivity were made on the right/left-handed polarization receiving systems at multiple wavebands in the whole elevation range, the continuum measurement bandwidth was 512 MHz, and the spectral resolution was 1 MHz, commonly the power detection band-

width of 20 MHz and the integration time of 1 s were adopted, but at the L and S bands with more interferences existed, the 5 MHz or narrower bandwidth was adopted. For the X and C wavebands and all the different elevation angles, the measurements were made respectively under the servo-controlled and fixed subreflector two cases. In each case, the cross-scan method was adopted at first to calibrate the pointing accuracy, so as to correct the residual error of the pointing model in the whole sky, and to ensure that in the process of measurement, the pointing error is within 1/10 beam width, then by pointing the antenna to the radio source, deviating it from the radio source, and igniting the noise source, finally, the variation of integrated power with the time similar with Fig.3 was obtained. Besides, for the C-band broad band receiver of 4∼8 GHz, we made the performance measurements at three frequency points, in favor of the efficiency correction in astronomical observations. For the subreflector servo, the models of Eqs.(11-12), namely the control model in the gravity direction Y and the control model in the focusing direction Z, were adopted:

$$Y = A + B\cos\varphi, \tag{11}$$

$$Z = C + D\sin\varphi, \tag{12}$$

in which A, B, C, and D are the fitted coefficients. The model simulation and actually measured curves are given in Figs.5∼6, in which, the model simulation adopted the finite element model of the 54th Research Institute of China Electronic Technology Group Company, and the measured data were obtained by using the radio source method.

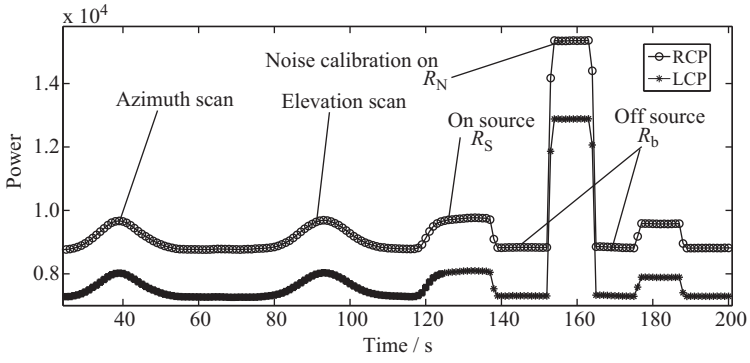

Fig. 4 The flux curve of a calibration radio source

5.2.1 Antenna Efficiency Measurement

In the measurement, the calibration sources 3C48, 3C147, 3C286, 3C295, and 3C138 etc. were selected, their flux densities at the L, C, S, and X bands are all greater than 3 Jy, they are stable, and able to be accurately calculated, besides, they are compact with a small angular size. In order to obtain the efficiency (as same as the sensitivity and system noise

temperature) in the whole elevation range, multiple measurements were made at different elevation angles. Table 2 gives the fitted parameters of the efficiency curves with respect to the elevation angle at four frequency bands when the subreflector is fixed. Table 3 gives the fitted parameters of the efficiency curves with respect to the elevation angle at the C and X bands, as well as the optimal efficiency values and their corresponding elevation angles, when the subreflector is servo-controlled. Figs.7∼12 show respectively the variations of efficiency with the elevation angle at the four wavebands, in Fig.7 VP expresses the vertical polarization, and HP means the horizontal polarization. We can find that at the L and S bands the variations of efficiency with the elevation are not apparent, but it is very significant at the X band, because that the effect of the deformation of subreflector supporting is more serious at the high-frequency band, as shown by Fig.9, in which LCP means the left-handed polarization, RCP means the right-handed polarization, LCP-SR and RCP-SR indicate respectively the left-handed and right-handed polarizations under the condition of servo-controlled subreflector. We can find that when the subreflector is fixed, the reduction of efficiency is very significant at low and high elevations, at the 10° and 85° elevations the efficiency decreases about 25%, and that after the subreflector is servo-controlled, the antenna efficiency can be controlled to be over 60% in the whole elevation range. Figs.10∼12 show the measured efficiency curves at the different frequencies in the C band, the antenna efficiency reduces apparently at the low and high elevations, and Figs.13∼14 show the fitted results before and after the subreflector is servo-controlled. It is noteworthy that in theory, the efficiency curves of the left-handed and right-handed polarizations should be identical, but in practical measurements the calibration error of the noise source will cause a difference of the two efficiency curves. As shown by Figs.13∼14, the maximum difference of about 4% between the LCP and RCP efficiency curves appears at 7.5 MHz, according to the analysis of Sec.3.1, the corresponding calibration error is ∼0.5 K (when the calibration noise temperature is 10 K, the relative calibration error is 5%), and at other two frequencies the LCP and RCP efficiency curves are coincident well, the efficiency difference is less than 1%, from which the estimated calibration error is less than 0.13 K (for the calibration noise temperature of 10 K, the relative calibration error is better than 2%), further more, the LCP and RCP efficiency curves vary with the elevation in a similar manner, this can be verified from Figs.13∼14.

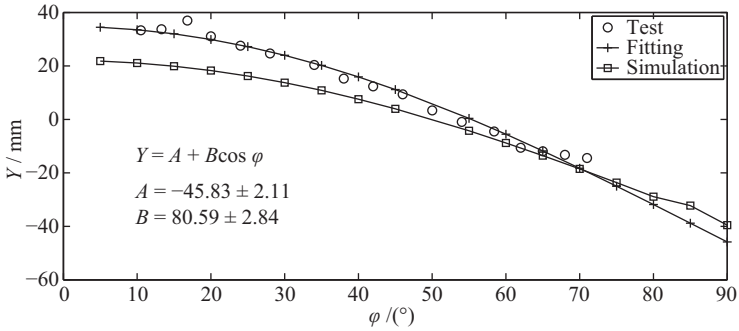

Fig. 5 The subreflector servo model in the Y direction

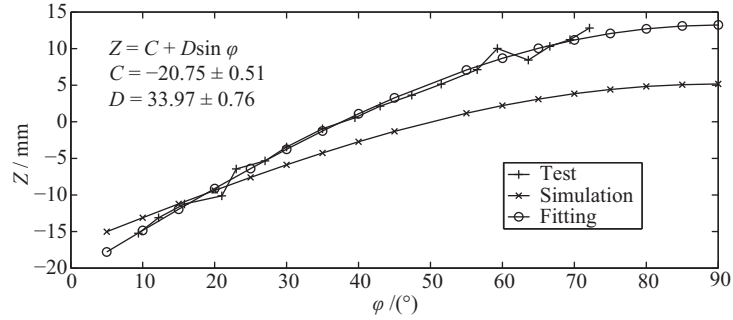

Fig. 6 The subreflector servo model in the Z direction

Table 2 The measured efficiency curves at four frequency bands when the subreflecfor is fixed

Band	Frequency /MHz	DPFU /(K/Jy)	Efficiency max	a	b	c	d
L(V)	1488	0.768	0.64@ $\varphi = 46.4$	1.6×10^{-6}	-3.6247×10^{-4}	0.02326739	0.54048039
L(H)	1488	0.796	0.66@ $\varphi = 43.4$	2.05×10^{-6}	-3.565×10^{-4}	0.01929101	0.66628028
S(LCP)	2200	0.714	0.59@ $\varphi = 10.2$	-9.4×10^{-7}	1.4481×10^{-4}	−0.00814504	1.06917228
S(RCP)	2200	0.662	0.55@ $\varphi = 10.2$	1.5×10^{-7}	-2.727×10^{-5}	−0.00021980	1.00494185
C(LCP)	4800	0.759	0.63@ $\varphi = 39.8$	1.24×10^{-6}	-3.086×10^{-4}	1.864331×10^{-2}	0.66883624
C(RCP)	4800	0.781	0.65@ $\varphi = 39.8$	1.45×10^{-6}	-3.4303×10^{-4}	2.041594×10^{-2}	0.63969328
C(LCP)	6425	0.716	0.60@ $\varphi = 42.1$	1.49×10^{-6}	-4.304×10^{-4}	2.853933×10^{-2}	0.45049085
C(RCP)	6425	0.700	0.58@ $\varphi = 46.6$	1.67×10^{-6}	-4.5683×10^{-4}	2.969396×10^{-2}	0.43482568
C(LCP)	7500	0.696	0.55@ $\varphi = 46.6$	8.3×10^{-7}	-3.9777×10^{-4}	3.179685×10^{-2}	0.29843024
C(RCP)	7500	0.663	0.55@ $\varphi = 46.6$	9.2×10^{-7}	-4.1208×10^{-4}	3.233525×10^{-2}	0.29487628
X(LCP)	8400	0.732	0.61@ $\varphi = 38.237$	2.97×10^{-6}	-6.9203×10^{-4}	0.04010060	0.31264468
X(RCP)	8400	0.722	0.60@ $\varphi = 38.909$	3.11×10^{-6}	-7.1699×10^{-4}	0.04161635	0.28315579

Note: in this table a, b, c, and d are the coefficients of the fitting polynomial $a\varphi^3 + b\varphi^2 + c\varphi + d$, in which the unit of φ is °.

Table 3 The measured efficiency curves at the C and X bands when the subreflector is servo-controlled

Band	Frequency /MHz	DPFU /(K/Jy)	Efficiency max	a	b	c	d
C(LCP)	4800	0.771	0.64@ $\varphi = 48.7$	6.4×10^{-7}	-1.1908×10^{-4}	7.05175×10^{-3}	0.86551495
C(RCP)	4800	0.785	0.65@ $\varphi = 47.1$	6.8×10^{-7}	-1.2899×10^{-4}	7.59555×10^{-3}	0.85688260
C(LCP)	6425	0.719	0.60@ $\varphi = 54.7$	3.0×10^{-8}	-3.028×10^{-5}	3.03171×10^{-3}	0.91954072
C(RCP)	6425	0.708	0.59@ $\varphi = 54.7$	1.5×10^{-7}	-4.839×10^{-5}	3.95895×10^{-3}	0.90378113
C(LCP)	7500	0.764	0.64@ $\varphi = 55.3$	1.7×10^{-7}	-6.686×10^{-5}	5.85544×10^{-3}	0.85217763
C(RCP)	7500	0.715	0.60@ $\varphi = 56.9$	9.0×10^{-8}	-5.493×10^{-5}	5.37263×10^{-3}	0.85531771
X(LCP)	8400	0.789	0.66@ $\varphi = 60.1$	-1.99×10^{-6}	2.4240×10^{-4}	-0.00757999	1.01166495
X(RCP)	8400	0.782	0.65@ $\varphi = 60.9$	-1.99×10^{-6}	2.4415×10^{-4}	-0.00763073	1.00900602

Note: in this table a, b, c, and d are the coefficients of the fitting polynomial $a\varphi^3 + b\varphi^2 + c\varphi + d$, in which the unit of φ is °.

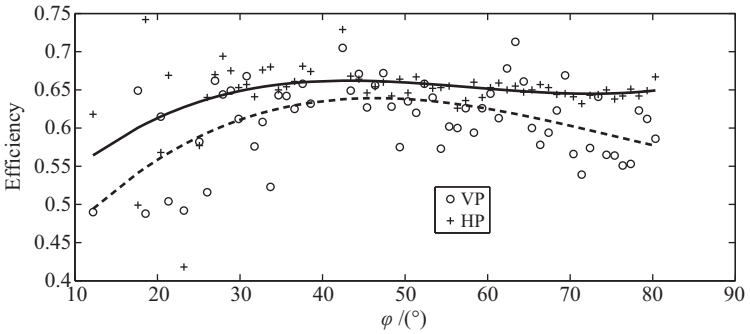

Fig. 7 The L-band efficiency measured at 1.488 GHz with a 2 MHz bandwidth and the radio source 3C123

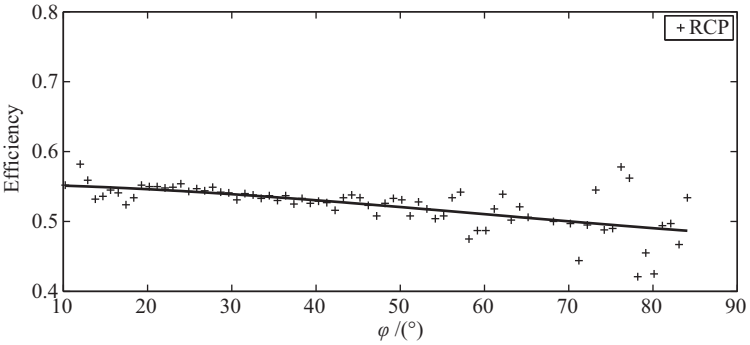

Fig. 8 The S-band RCP efficiency measured at 2.2 GHz with a 20 MHz bandwidth and the radio source 3C123

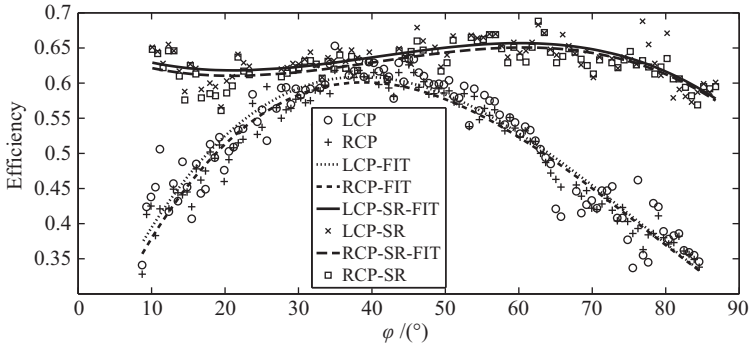

Fig. 9 The X-band LCP and RCP efficiencies measured at 8.4 GHz with a 20 MHz bandwidth and the radio source 3C286

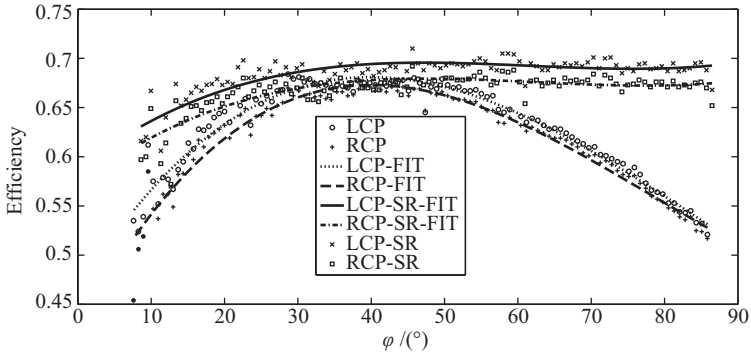

Fig. 10 The C-band LCP and RCP efficiencies measured at 4.8 GHz with a 20 MHz bandwidth and the radio sources 3C286 and 3C123

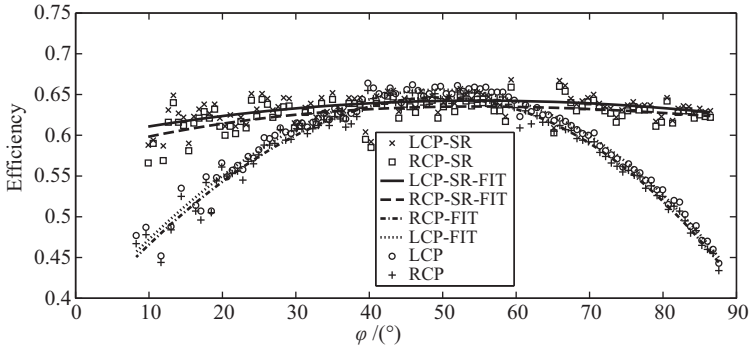

Fig. 11 The C-band LCP and RCP efficiencies measured at 6.425 GHz with a 20 MHz bandwidth and the radio sources 3C286 and 3C123

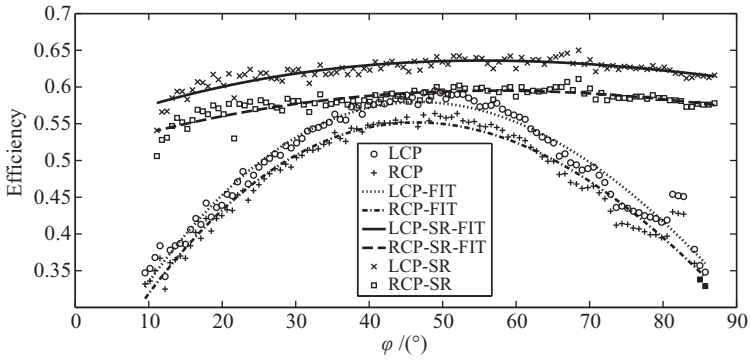

Fig. 12 The C-band LCP and RCP efficiencies measured at 7.5 GHz with a 20 MHz bandwidth and the radio sources 3C286 and 3C123

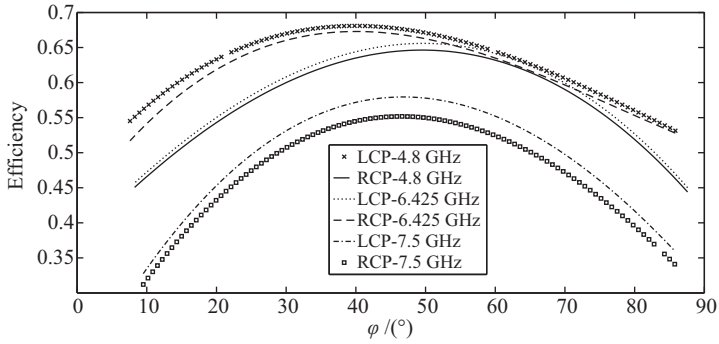

Fig. 13 The curves of C-band LCP and RCP efficiencies when the subreflector is fixed

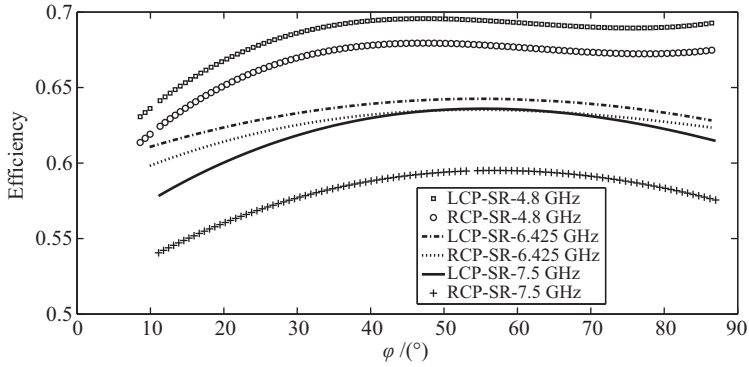

Fig. 14 The curves of C-band LCP and RCP efficiencies when the subreflector is servo-controlled

5.2.2 Sensitivity Measurement

Figs.15∼18 give the measurements of SEFD at four wavebands, at low elevation angles, because of the increased system noise temperature, the SEFD becomes large (i.e., the sensitivity declines); at high elevation angles, the SEFD becomes also large, because of the reduced efficiency.

As the measuring error of SEFD does not depend on the calibration error of the noise source, hence it is necessary to study the sensitivities at different frequencies for the waveband with a broad frequency coverage. Fig.19 presents the RCP sensitivities at 4 800 MHz, 6 425 MHz, and 7 780 MHz three C-band frequencies, from this figure we can find that at each elevation, the corresponding sensitivity declines with the increasing frequency, and that at the 55° optimal elevation, the SEFDs at the three frequencies are identical, all are about 27 Jy. When the subreflector is servo-controlled, the sensitivities at the three frequencies vary with the elevation consistently. Figs.20∼21 show the variations of SEFD with the elevation at the C and X bands when the subreflector is servo-controlled, we can find that the SEFDs at the high and low elevations have a rather large improvement because of the servo control of the subreflector, the X-band SEFD has improved for 100%, and the C-band SEFD has improved for about 1/3.

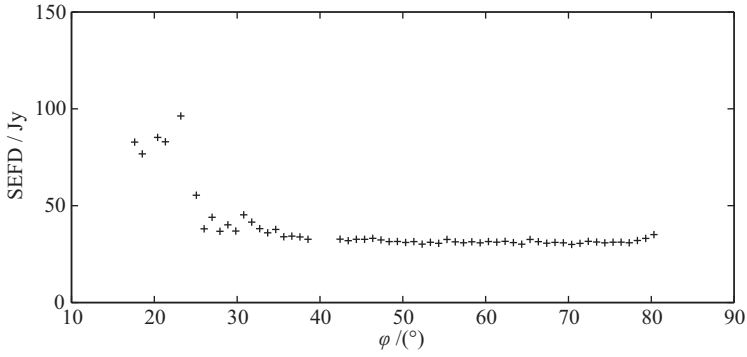

Fig. 15 The L-band SEFD measured at 1.488 GHz with a 2 MHz bandwidth and the radio source 3C123

5.2.3 Measurement of system noise temperature

Fig.22 gives the measurement of RCP system noise temperatures at four frequency bands (the L band is of horizontal polarization), at high elevations the X-band system noise temperature is ∼31 K, the C-band system noise temperature is 20K̇, S-band is ∼55 K, and L-band is 25 K, the system noise temperature at the S band tends to be large, this is caused by the extremely bad radio environment on the site of the TM65m antenna, and the global enhancement of the sky noise at this waveband.

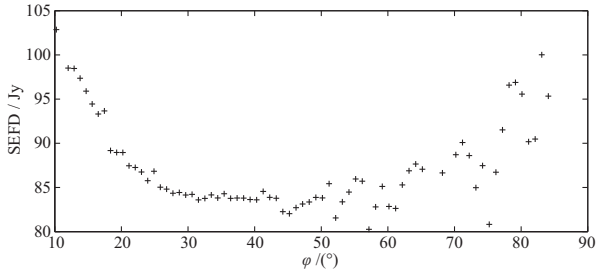

Fig. 16 The S-band RCP SEFD measured at 2.2 GHz with a 20 MHz bandwidth and the radio source 3C123

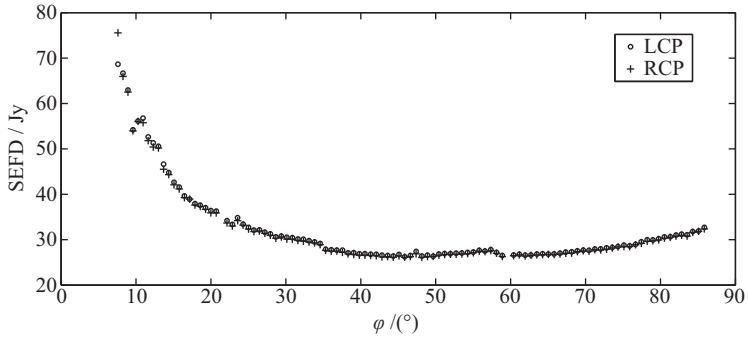

Fig. 17 The C-band LCP and RCP SEFDs measured at 4.8 GHz with a 20 MHz bandwidth and the radio source 3C286

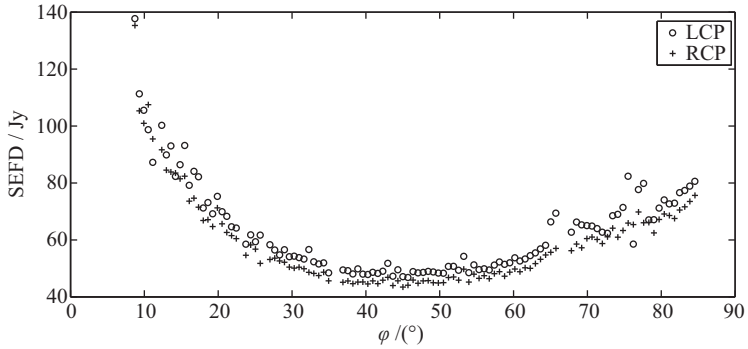

Fig. 18 The X-band LCP and RCP SEFDs measured at 8.4 GHz with a 20 MHz bandwidth and the radio source 3C286

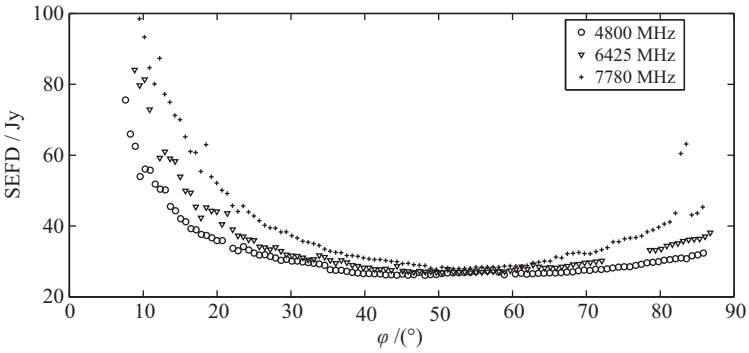

Fig. 19 The variations of C-band RCP SEFD with the elevation measured at three frequencies

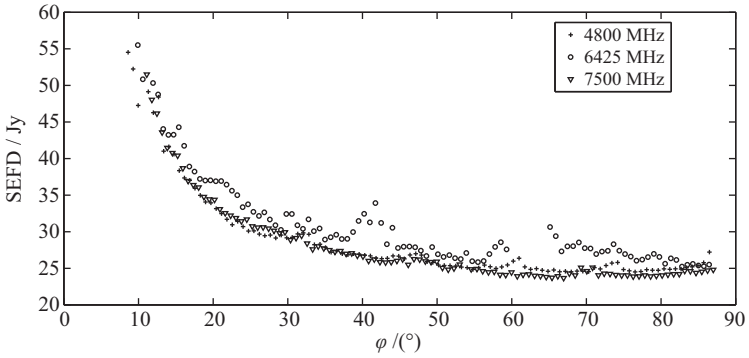

Fig. 20 The variations of C-band RCP SEFD with the elevation measured at three frequencies when the subreflector is servo-controlled

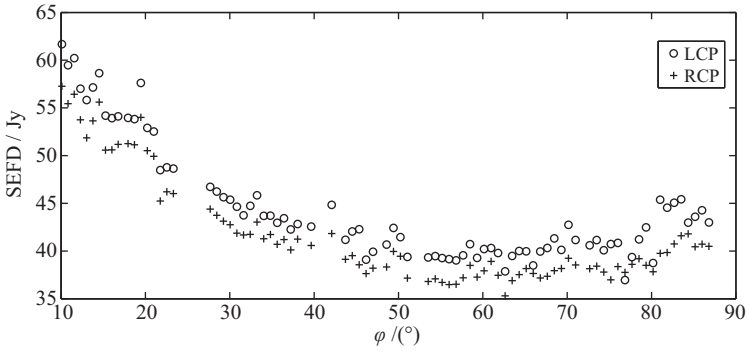

Fig. 21 The variations of X-band LCP and RCP SEFDs with the elevation when the subreflector is servo–controlled

Fig.23 shows the curves of C-band system noise temperatures at 7.5 GHz before and after the subreflector is servo-controlled, the two tests were all made in cloudy weather, from which we can find that the subreflector servo has no significant influence on the system noise temperature. Fig.24 shows the measurements of X-band system noise temperatures at 8.4 GHz before and after the subreflector is servo-controlled, the weathers of the two measurements have a rather large difference, the measurement when the subreflector is fixed was made on the cloudy day, while the measurement when the subreflector is servo-controlled was made on a fine day, we can find that the two measurements have a systematic difference of about 2.5 K, this should be attributed to the difference of atmospheric conditions, but the relative difference between the LCP and the RCP keeps to be fine, with a difference of about 3 K. Since the measurement of system noise temperature relates quite with the atmospheric condition, here we can take the data obtained at the same time but different frequencies to make comparisons. At present the maximum bandwidth of our data sampling back end is 500 MHz, Fig.25 gives the curves of the system noise temperatures on the continuous 500 MHz bandwidths at three frequencies, we can find that the system noise temperature increases with the increasing frequency, and that the increment of system noise temperature is linearly proportional to the frequency separation (Note: the data around the 83° elevation are the abnormal points of the measurement caused by the mistake of the antenna scanning velocity, after the scanning velocity being adjusted to normal values, the data of 84°∼86° elevations become normal).

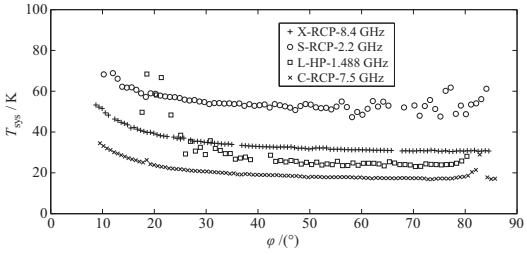

Fig. 22 The system noise temperatures at four wavebands

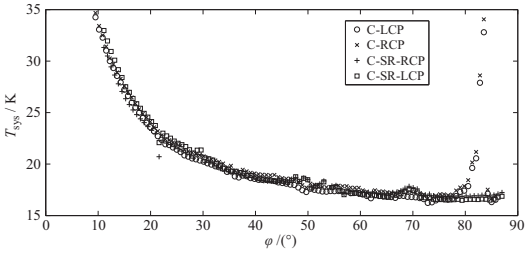

Fig. 23 The C-band (7.5 GHz) system noise temperatures before and after the subreflector is servo-controlled

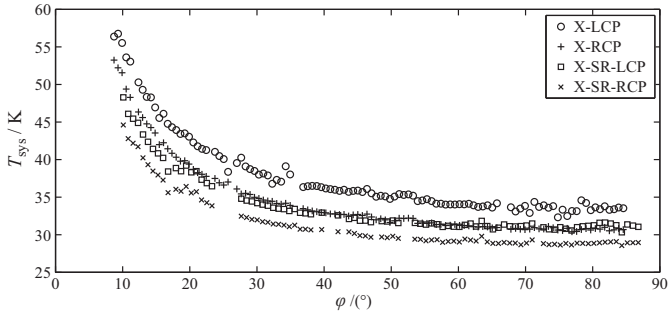

Fig. 24 The C-band (8.4 GHz) system noise temperatures before and after the subreflector is servo-controlled

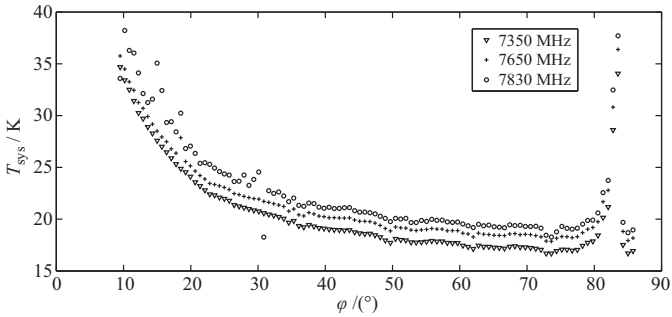

Fig. 25 The C-band RCP system noise temperatures measured simultaneously at three frequencies

6. SUMMARY

This paper has discussed particularly the performance measurements of the four low-frequency receiving systems installed on the TM65m radio telescope, and given the measured results at the C and X bands under the condition of servo-controlled subreflector. The measured results indicate that at the optimal elevation all the efficiencies at the L, S, C, and X four bands can attain 60% or higher, the sensitivity SEFDs are respectively about 30 Jy, 83 Jy, 25 Jy, and 40 Jy, after the subreflector servo is activated, the efficiencies of the C and X bands at all elevation angles can be over 60%, and the SEFDs at low and high elevations have a 2-fold improvement; at the optimal elevation, the system noise temperatures at the four wavebands are respectively about 26 K, 57 K, 20 K, and 32 K, and for both C and X bands the activation of subreflector servo has no significant influence on the system noise temperature.

At present, the major factor causing the uncertainty of the efficiency measurement is the calibration error of the noise source, which is now about 2%, at some frequency points it can attain 5%, but even so this has been improved for over two times than the error of laboratory calibration. In order to improve the accuracies of the efficiency and system noise temperature measurements, to make efforts in the following aspects seems to be valuable:

(1) In measurements, it is found that along with the variation of antenna elevation, especially at low and high elevations, the antenna pattern deforms significantly, this causes the side-lobe energy to increase and the main-beam energy to decrease, and finally the reduction of the measured value of antenna efficiency. Hence, it is necessary to build up a relation between the characteristics of antenna directivity pattern and the elevation;

(2) To make a precise temperature control on the noise source, in order to improve the stability of the noise source and the calibration accuracy;

(3) The disk source has a very large flux value, and can suppress effectively noises, even a short time integration can result in a fine signal to noise ratio, so it is very favorable to the measurement, but the error of beam correction factor of a disk source is quite large, and therefore it will cause the increase of uncertainty. Alternatively, by scanning the 2-dimensional antenna pattern we can make the power integration of the whole antenna pattern, and derive the antenna performance from the integrated power, thus the problem of correction factor of a disk source can be avoided.

References

1 Baars M., Genzel R., Pauliny K., et al., A&A, 1997, 61, 99

2 Klein M., Stelzried T., AJ, 1976, 81, 1078

3 Baars J. W. M., ITAP, 1973, 21, 461

4 Ulich B. L., Haas R. W., ApJS, 1976, 30, 247

5 Wang J. Q., Yu L. F., Zhao R. B., et al., AcASn, 2015, 56, 63

6 Qian Z. H., Li J. L., Application of VLBI Technique in Deep Space Explorations, Beijing: China Science and Technology Press, 2014, 33

7 Ott M., Witzel A., Quirrenbach A., et al., A&A, 1994, 284, 331

8 Wang J. Q., Yu L. F., Zhao R. B., et al., Scientia Sinica G, 2014, 44, 1232

9 Smith P., ITAP, 1966, 14, 6